Supplementary Information (SI) for Chemical Science.
This journal is © The Royal Society of Chemistry 2024

High Entropy Metallic-High Entropy Nonmetallic Community as High Performance Electrocatalysts for Oxygen Evolution Reaction and Oxygen Reduction Reaction

Chunyan Zhang,[a] Hang Li,[a] Mengfei Su,[a] Shengfa Li,[a] Feng Gao,[b]* and Qingyi Lu[a]*

[a] State Key Laboratory of Coordination Chemistry, Coordination Chemistry Institute, Collaborative Innovation Center of Advanced Microstructures, School of Chemistry and Chemical Engineering, Nanjing University, Nanjing 210023, P. R. China. E-mail: qylu@nju.edu.cn

[b] Department of Materials Science and Engineering, Jiangsu Key Laboratory of Artificial Functional Materials, Collaborative Innovation Center of Advanced Microstructures, College of Engineering and Applied Sciences, Nanjing University, Nanjing 210023, P. R. China. E-mail: fgao@nju.edu.cn

Experimental

Chemicals and materials: Raw chemical materials including cobalt chloride ($CoCl_2 \cdot 6H_2O$, AR, ≥ 98%), nickel chloride ($NiCl_2 \cdot 6H_2O$, AR, ≥ 98%), iron(III) nitrate ($Fe(NO_3)_3 \cdot 9H_2O$, AR, ≥ 98%), manganese chloride ($MnCl_2 \cdot 4H_2O$, AR, ≥ 98%), chromic chloride ($CrCl_2 \cdot 6H_2O$, AR, ≥ 98%), urea (AR, ≥ 99%), aminotriazole (AR, ≥ 98%), sodium hypophosphite, thiourea, polyvinylpyrrolidone (K30, PVP, AR, ≥ 99%) were purchased from Shanghai Macklin Biochemical Co., Ltd. All the reagents were used directly without further purification.

Synthesis of the high entropy metal precursor: Firstly, 25 mL DMF, 2 mL deionized water and 2 mL ethyl alcohol were mixed and stirred well to form a uniform solution. Secondly, equimolar amount of 0.5 mmol of cobalt chloride, nickel chloride, iron (III) nitrate, manganese chloride, and chromic chloride, 0.5 g of urea and 0.5 mmol aminotriazole were added into the above solution, forming a stable dispersion. The mixed solution was subsequently transferred into a 50 mL Teflon-lined stainless-steel autoclaves that were heated at 120 °C for 8 h. After the autoclave was cooled to room temperature, the precursors were collected by centrifuging several times with ethanol and deionized water and drying at 80 °C for 6 h.

Synthesis of the (MnFeCoNi)-precursor and the (FeCoNi)-precursor: The synthesis of (MnFeCoNi)-precursor or (FeCoNi)-precursor is the same as that of the high-entropy metal precursor, except that the corresponding metal salts are selectively added. For the synthesis (MnFeCoNi)-precursor, the added salts are manganese chloride, ferric nitrate, cobalt chloride and nickel chloride. When synthesizing (FeCoNi)-precursor, the metal salts added are ferric nitrate, cobalt chloride and nickel chloride.

Synthesis of the HEM-HENMC: The upstream gas method was used to prepare the HEM-HENMC. Firstly, the 0.5 g of $Na_2HPO_2 \cdot H_2O$ and 0.5 g thiourea were put on the upstream end and 0.2 g of the as-prepared high entropy metal precursor was put on the downstream end of the tube furnace. Subsequently, the tube furnace was heated to 450 °C at a heating rate of 2 °C min^{-1} and kept for for 2 h under a N_2 atmosphere. After the simultaneous vulcanization and phosphatization process, the resultant product was washed with deionized water and dried at 60 °C under vacuum for 6 h, which was named as HEM-HENMC. The synthesis conditions for (MnFeCoNi)-P/S, (FeCoNi)-P/S, (CrMnFeCoNi)-N_2, (CrMnFeCoNi)-P, (CrMnFeCoNi)-S and (CrMnFeCoNi)-O_2 are

similar to the synthesis of HEM-HENMC, except the different calcination atmospheres as detailed in Table S1.

Characterizations: The products' X-ray diffraction (XRD) patterns were collected on a Bruker D8 ADVANCE diffractometer with Cu K_α radiation. Scanning electron microscopy (SEM) images were obtained on a Hitachi S-4800 scanning electron microscope with an accelerating voltage of 10 kV. Transmission electron microscope (TEM) and element mapping were acquired on JEM-2800 Plus with an electron acceleration energy of 200 kV. X-ray photoelectron spectroscopy (XPS) (PHI 5000 versa probe type) was used to characterize the chemical environment of the elements in the samples.

Electrochemical OER measurements: Electrochemical measurements were performed in a standard three-electrode cell in an electrolyte of 1 M KOH (90 %, reagent grade, Shanghai Macklin Biochemical Co., Ltd.) interfaced with a CHI760E electrochemical analyzer (CH Instruments, Inc., Shanghai). Before every measurement, the cell was thoroughly rinsed with pre-boiled DI water. A carbon rod and an Hg/HgO electrode were used as the counter and reference electrodes, respectively. Working electrodes were prepared as follows. Firstly, the catalyst ink was prepared by dispersing the catalyst (5 mg) in a mixed solvent (0.5 mL) containing 0.02 mL of a 5.0 wt.% Nafion solution and 1:3 (v/v) isopropanol/water. The ink was prepared by sonication for ≥30 min. Next, 40 μL of the ink was dropped onto a glassy carbon electrode with a diameter of 3 mm and the droplet was allowed to air-dry. The mass loading of the catalysts was about 0.14 mg cm^{-2}, calculated from the concentration and volume of the catalyst ink applied on the glassy carbon electrode. A commercial IrO_2 electrocatalyst was used to benchmark electrocatalyst performance (loading also 0.14 mg cm^{-2}). The linear sweep voltammetry (LSV) measurements were performed in an electrolyte of 1 M KOH, using a scan rate of 5 mV s^{-1}, in a potential range from 1.0 to 1.65 V versus reversible hydrogen electrode (RHE).

Electrochemical ORR measurements: The catalyst ink for ORR were prepared through the same way for OER. The ORR performances were also evaluated in 1 M KOH electrolyte using a three-electrode system. It included a rotating ring disk electrode (RRDE) as the working electrode, a carbon rod as the counter electrode, and a saturated Hg/HgO as the reference electrode. Before any tests, the 1 M KOH electrolyte was first saturated with O_2 or N_2 by purging with the appropriate

gas. The gas flow was maintained during the whole experiments. The linear sweep voltammetry (LSV) measurements were performed in O_2 or N_2 saturated electrolytes at rotating speeds ranging from 400 to 2500 rpm, using a scan rate of 5 mV s^{-1}. The accelerated durability tests for the HEM-HENMC were conducted by a constant voltage of 0.5 V in a 1 M O_2-saturated KOH solution. The final oxygen reduction currents were obtained by subtracting the background currents measured in the N_2-purged electrolyte from those measured in the O_2-saturated electrolyte. All potentials derived from the RRDE tests in 1 M KOH were converted to RHE potentials and corrected with 94% iR-compensation. All potential values were calibrated to the reversible hydrogen potential (E_{RHE}) based on the Nernst equation ($E_{RHE} = E_{GOE} + 0.095 + 0.0591 \times pH$). The H_2O_2 yield (% H_2O_2) and electron transfer number (n) were calculated using the following equations:

$$\%H_2O_2 = 200 \times \frac{I_R/N}{I_D + I_R/N} \quad \text{Se1}$$

$$n = 4 \times \frac{I_D}{I_D + I_R/N} \quad \text{Se2}$$

where I_D is the disk current, I_R is the ring current, and N is the collection efficiency of the ring electrode (0.37 in this work).

The electron transfer numbers for the oxygen reduction reaction were calculated from the linear slopes of J- versus ω-1/2 plots according to the Koutecký–Levich (K−L) equation:

$$\frac{1}{J} = \frac{1}{J_L} + \frac{1}{J_K} = \frac{1}{B\omega^{1/2}} + \frac{1}{J_K} \quad \text{Se3}$$

$$B = 0.62nFC_0(D_0)^{2/3}\upsilon^{-1/6} \quad \text{Se4}$$

$$J_K = nFkC_0 \quad \text{Se5}$$

where J is the measured current density, J_K is the kinetic current density, J_L is the diffusion-limited current density, ω is the angular velocity, n is the electron transfer number, F is the Faraday constant (96485 C mol^{-1}), C_0 is the bulk concentration of O_2 (1.15×10^{-6} mol cm^{-3}), D_0 is the diffusion coefficient of O_2 in 1 M KOH (1.6×10^{-5} cm^{-2} s^{-1}), υ is the kinetic viscosity of the electrolyte, and k is the electron transfer rate constant. Tafel slopes was also determined from the K-L equation.

Double-layer capacitance analyses: The electrochemical surface area (ECSA) was measured by cycling the electrode in the non-Faradaic regions under the same conditions used for catalysis

measurements. The double-layer capacitance of the electrode (C_{dl}, mF cm^{-2}) was estimated by the following equation:

$$J = \nu \times C_{dl} \quad \text{Se6}$$

Where, ν is the scan rate (V s^{-1}), J is the evolution of non-Faradaic current density (mA cm^{-2}).

$$ECSA = C_{dl}/C_{dlRef} \quad \text{Se7}$$

Where, C_{dlRef} is the double-layer capacitance of the electrode (C_{dlRef} = 40 µF cm^{-2}).

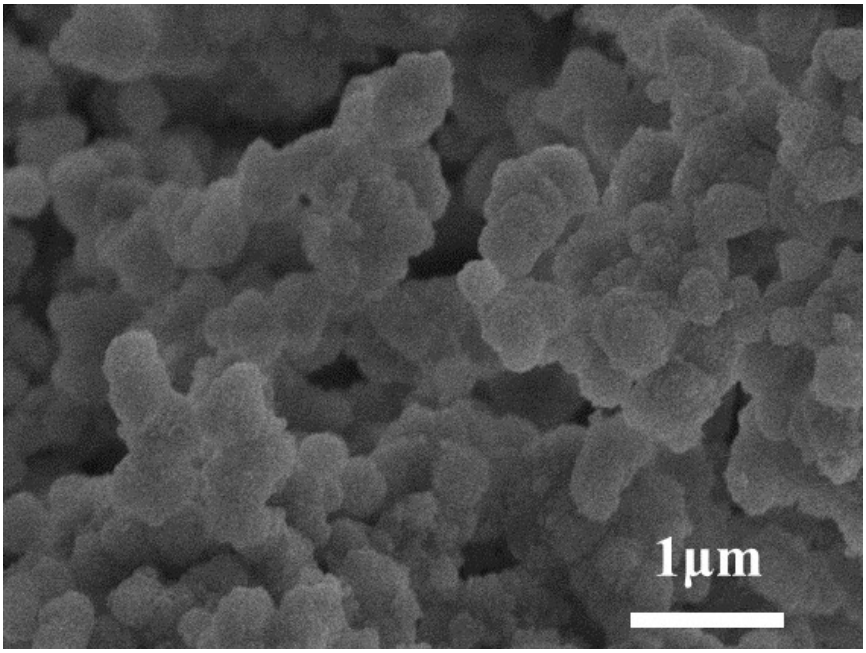

Figure S1. SEM image of HEM-HENMC.

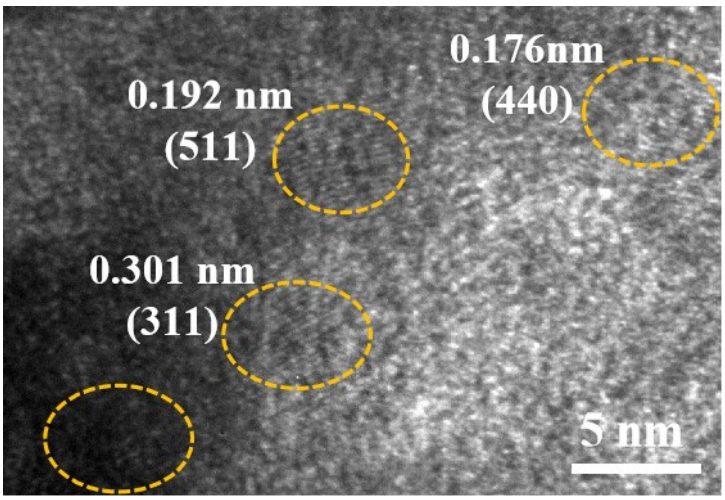

Figure S2. TEM image of HEM-HENMC.

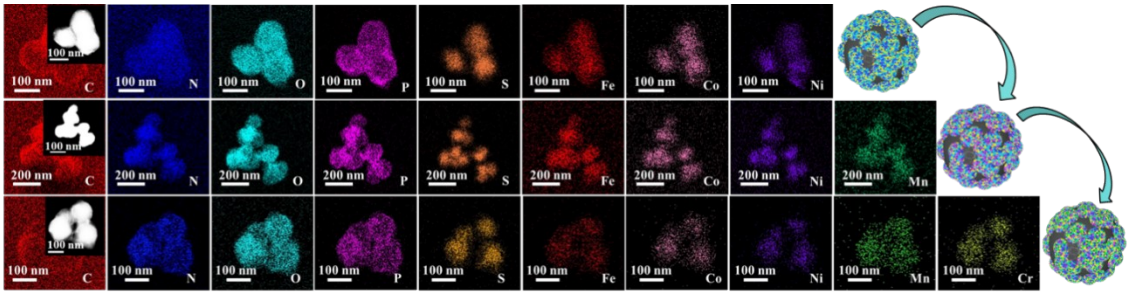

Figure S3. EDS elemental mappings for HEM-HENMC, quaternary (MnFeCoNi)-high entropy nonmetal system and ternary (FeCoNi)-high entropy nonmetal system.

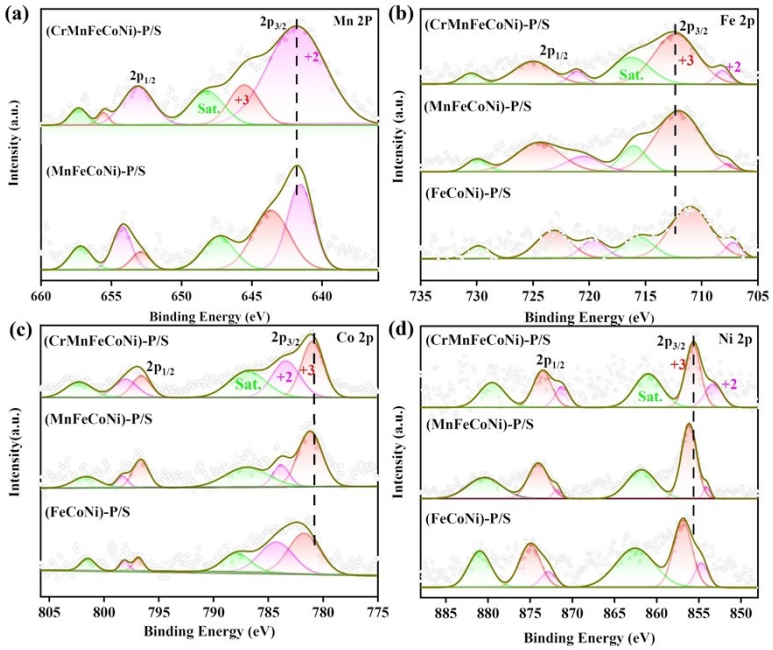

Figure S4. High resolution XPS spectra of HEM-HENMC, quaternary (MnFeCoNi)-high entropy nonmetal system and ternary (FeCoNi)-high entropy nonmetal system: (a) Mn 2p; (b) Fe 2p; (c) Co 2p and (d) Ni 2p.

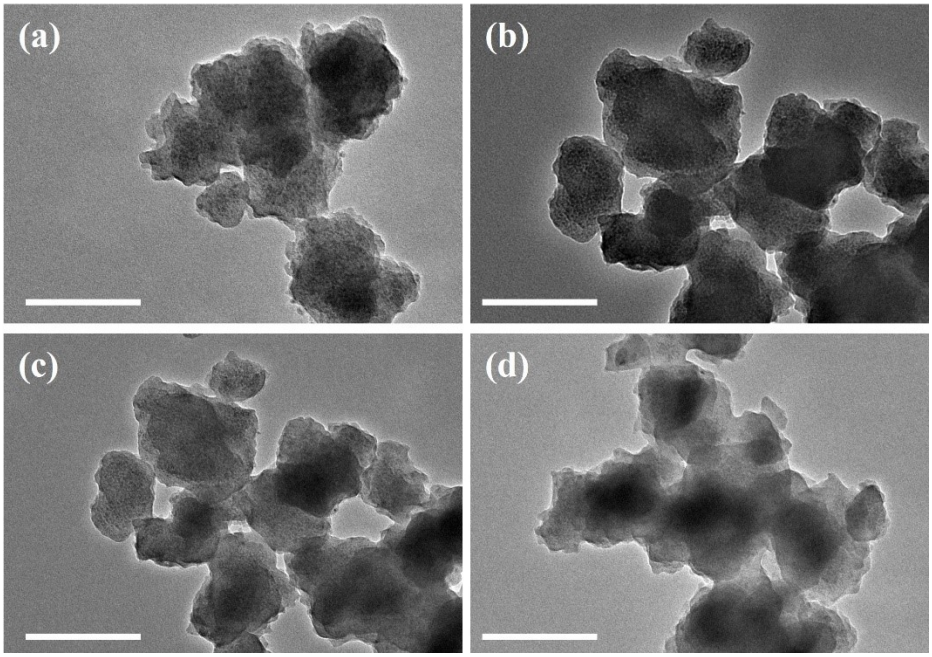

Figure S5. TEM images of (a) (CrMnFeCoNi)-P; (b) (CrMnFeCoNi)-N_2; (c) (CrMnFeCoNi)-S and (d) (CrMnFeCoNi)-O_2. The scale bars are 200 nm.

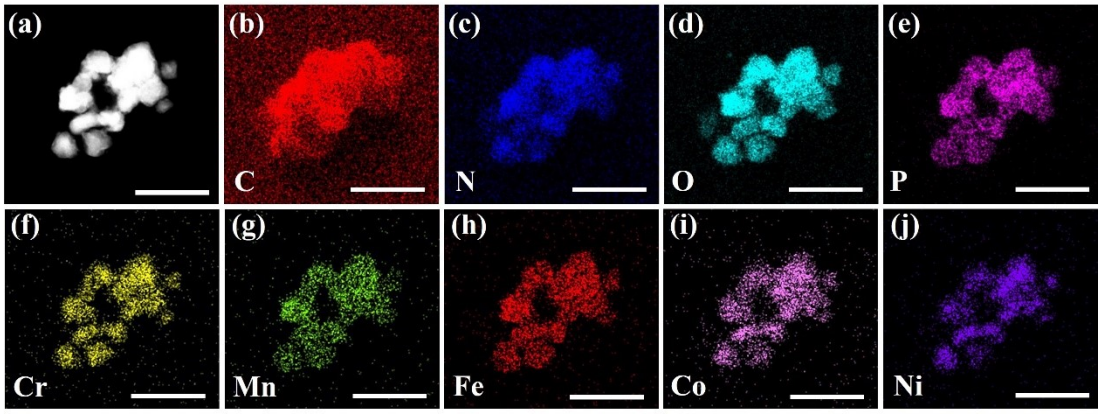

Figure S6. STEM-EDX elemental mappings of (CrMnFeCoNi)-P. The scale bars are 200 nm.

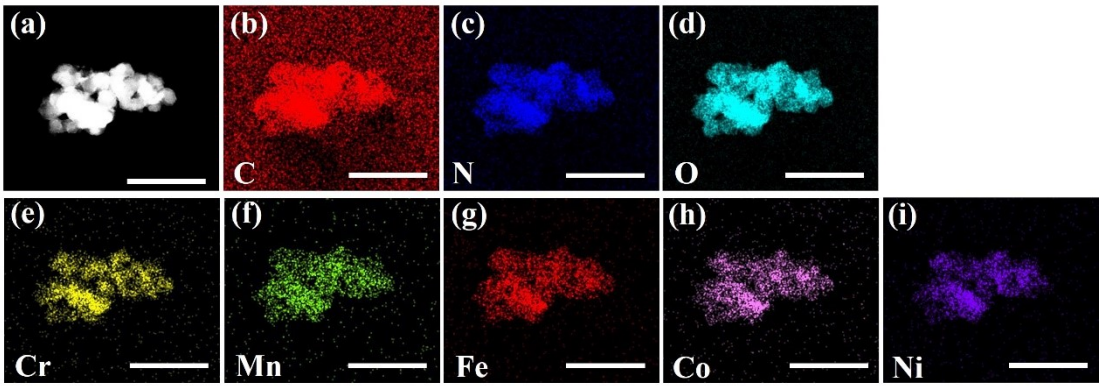

Figure S7. STEM-EDX elemental mappings of (CrMnFeCoNi)-N_2. The scale bars are 200 nm.

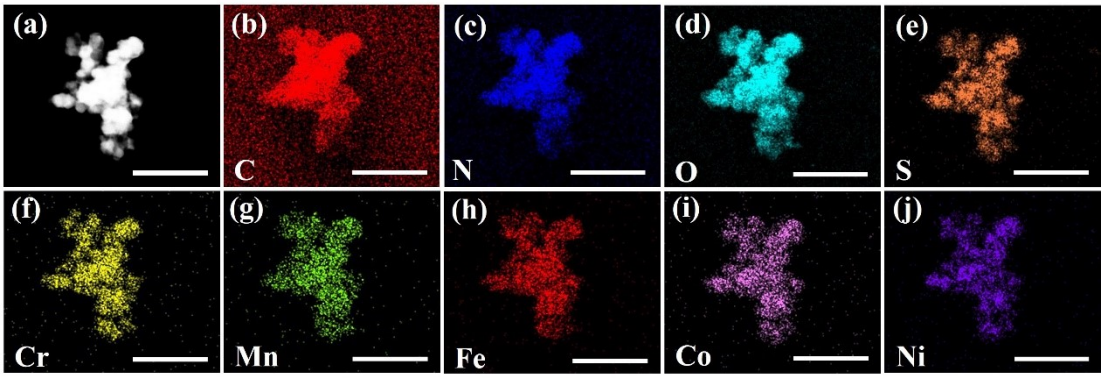

Figure S8. STEM-EDX elemental mappings of (CrMnFeCoNi)-S. The scale bars are 200 nm.

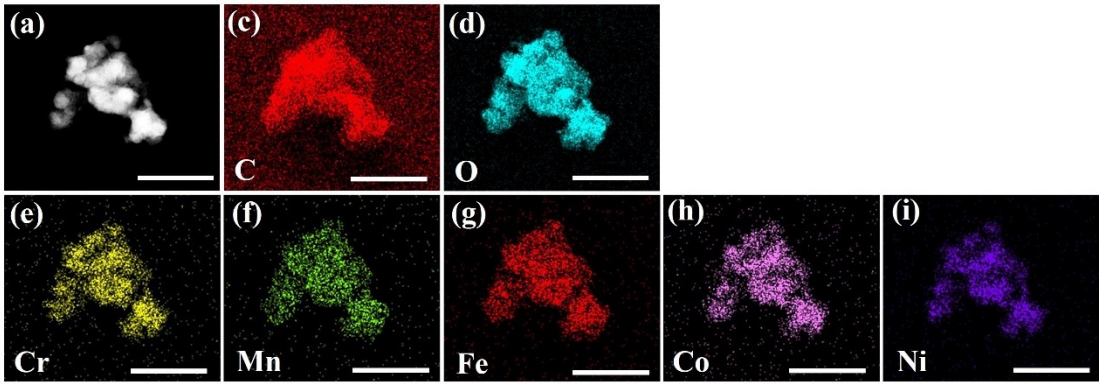

Figure S9. STEM-EDX elemental mappings of (CrMnFeCoNi)-O_2. The scale bars are 200 nm.

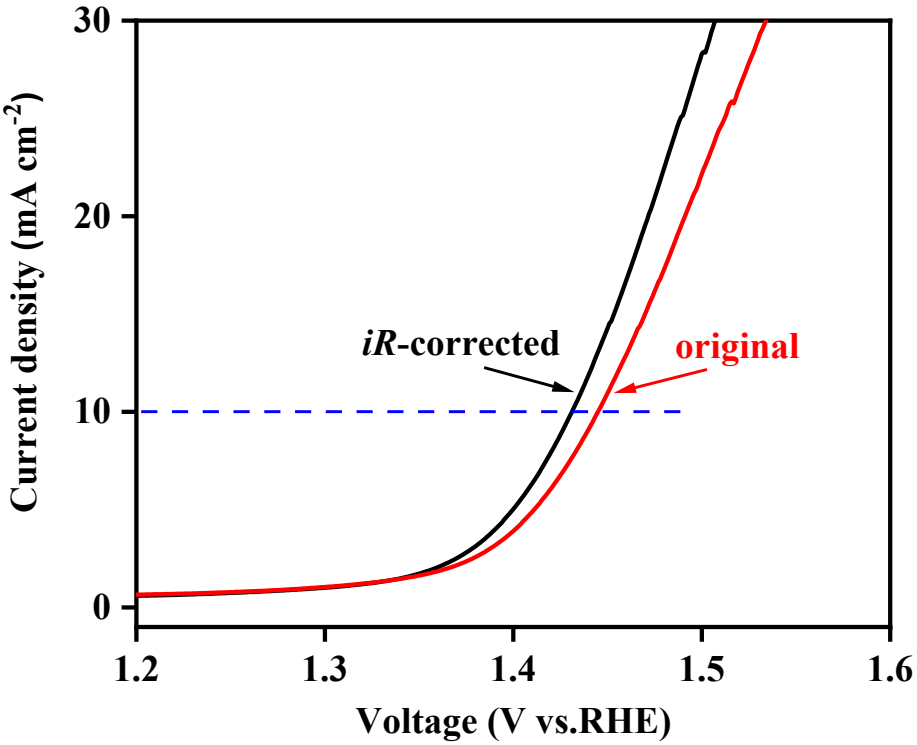

Figure S10. The original and iR-corrected LSV curves of HEM-HENMC.

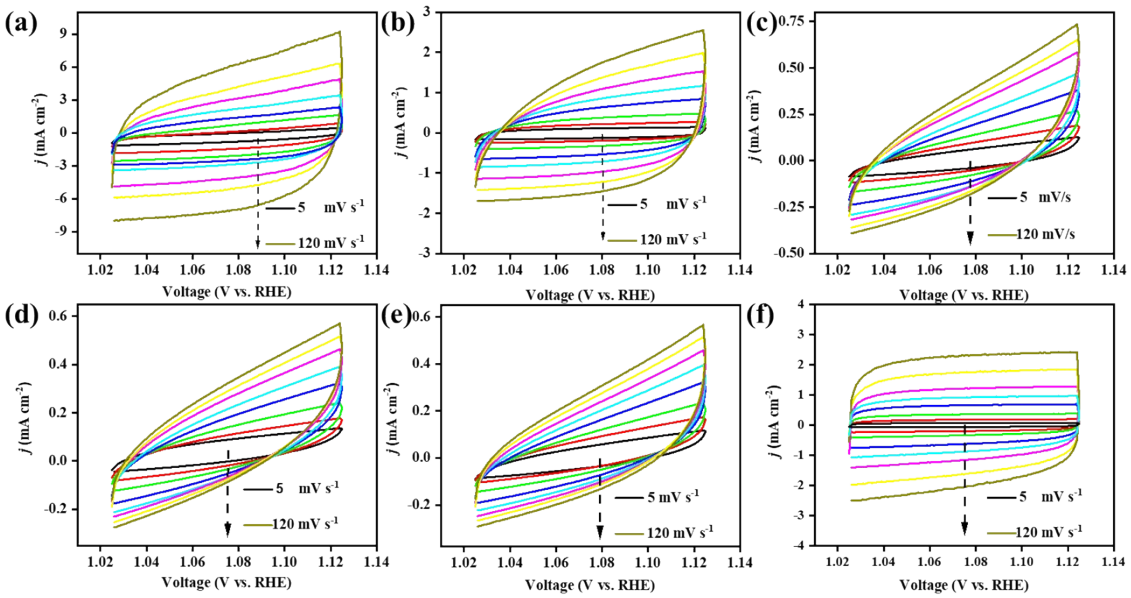

Figure S11. Cyclic voltammetry (CV) curves at various scan rates (5-120 mV s^{-1}) of (a) (CrMnFeCoNi)-P/S; (b) (CrMnFeCoNi)-P; (c) (CrMnFeCoNi)-S; (d) (CrMnFeCoNi)-N_2; (e) (CrMnFeCoNi)-O_2 and (f) IrO_2.

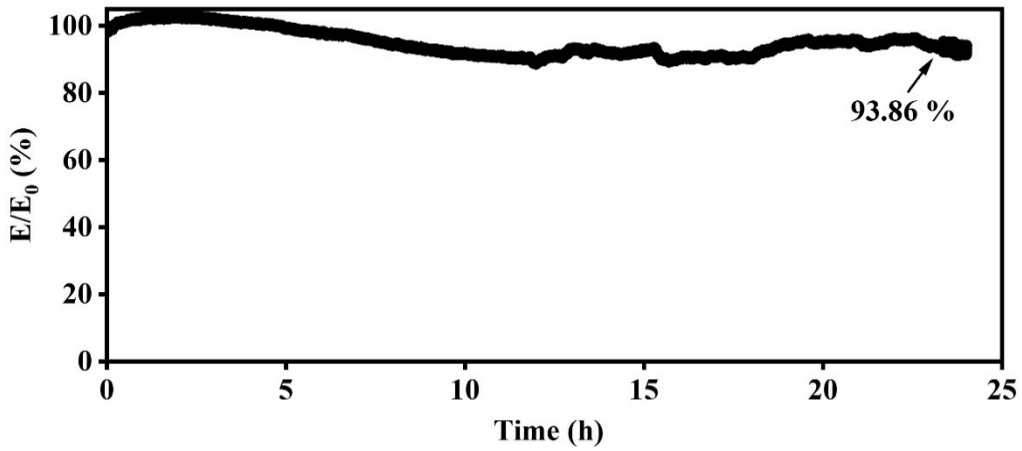

Figure S12. Long-time stability OER test of HEM-HENMC at a current density of around 60 mA cm^{-2} for 24 h.

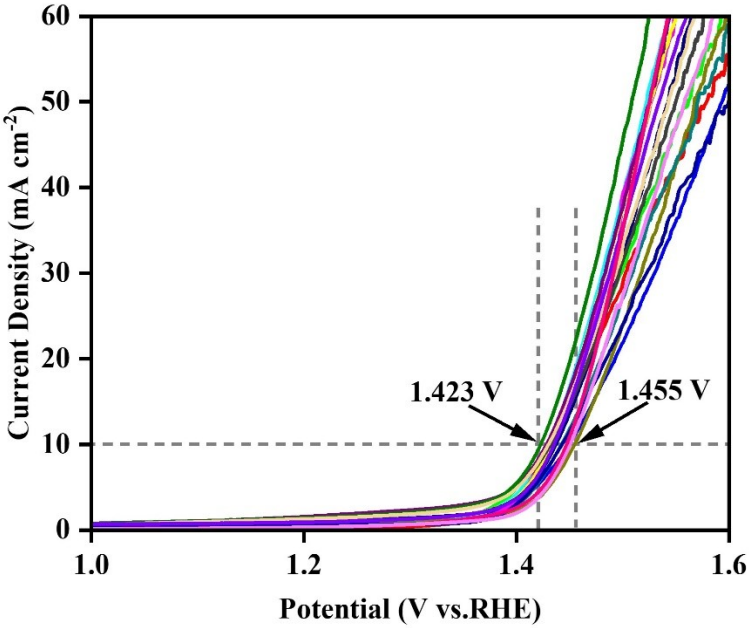

Figure S13. 20 OER polarization curves of HEM-HENMC from different synthetic batches.

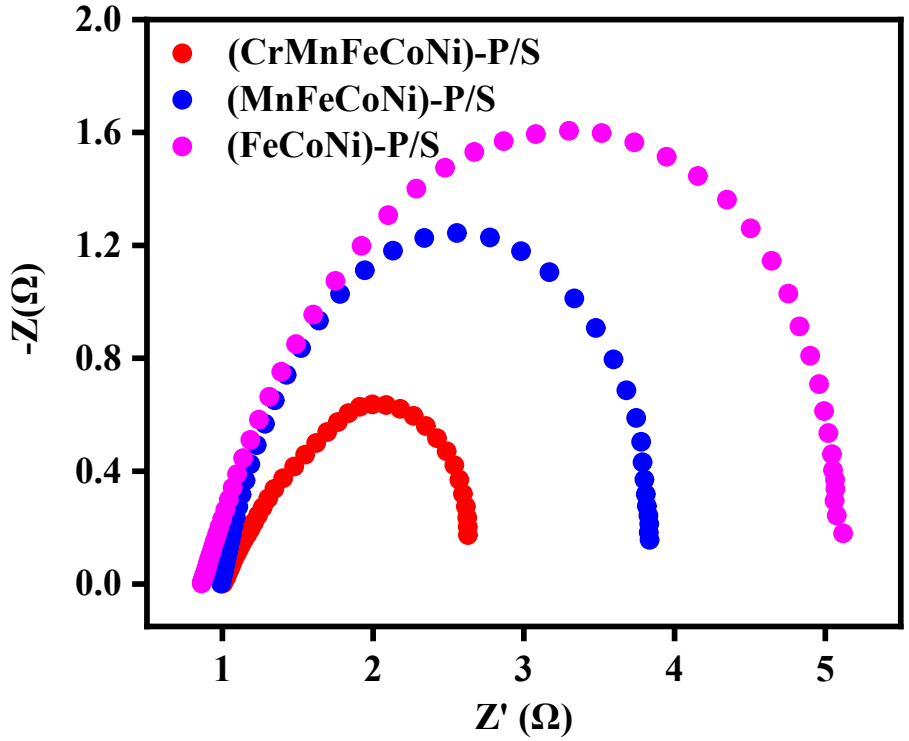

Figure S14. Electrochemical impendence spectra (EIS) of (CrMnFeCoNi)-P/S, (MnFeCoNi)-P/S and (FeCoNi)-P/S.

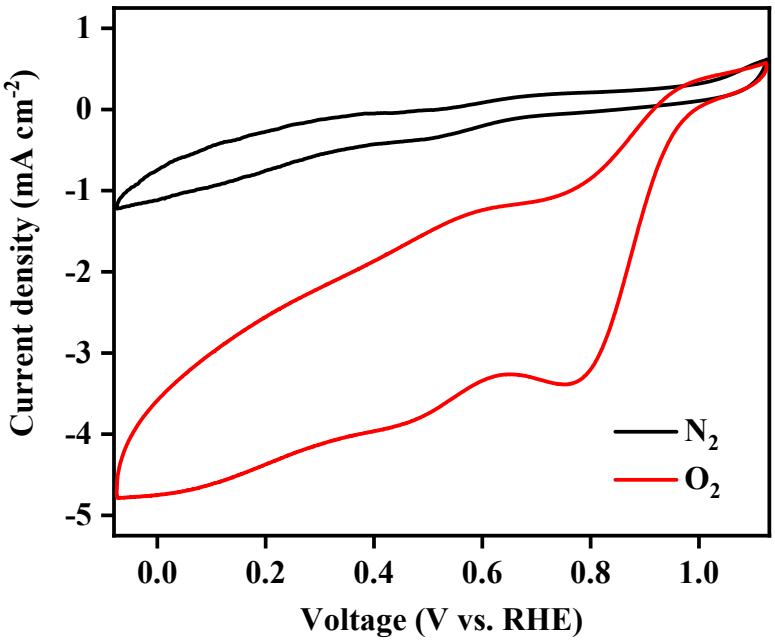

Figure S15. CV curves for HEM-HENMC in N_2 and O_2-saturated 1 M KOH (scan rate: 5 mV s^{-1}).

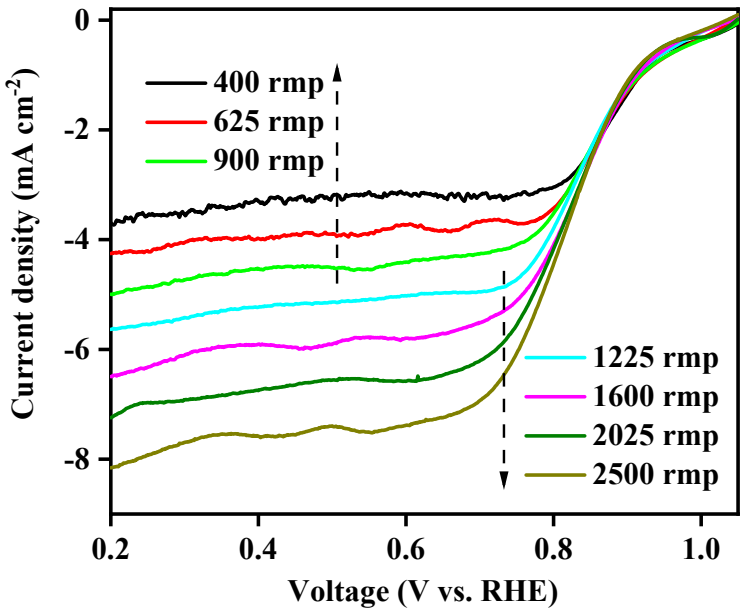

Figure S16. LSV curves of HEM-HENMC at different rotating speeds.

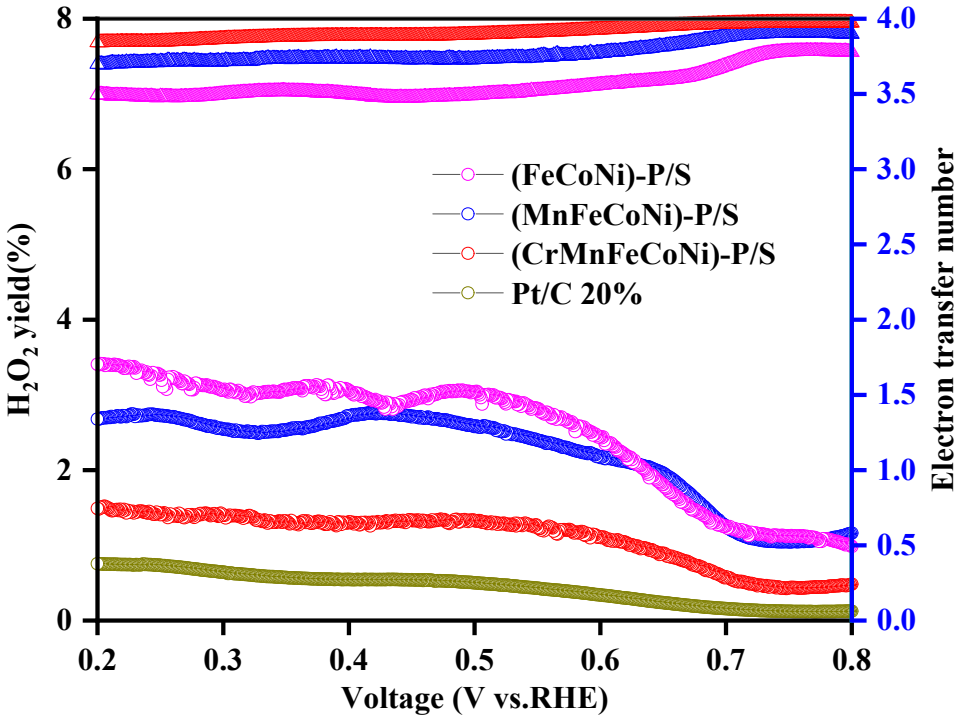

Figure S17. H_2O_2 yields and electron transfer number in ORR of the (CrMnFeCoNi)-P/S, (MnFeCoNi)-P/S, (FeCoNi)-P/S and commercial Pt/C 5 wt.% catalysts.

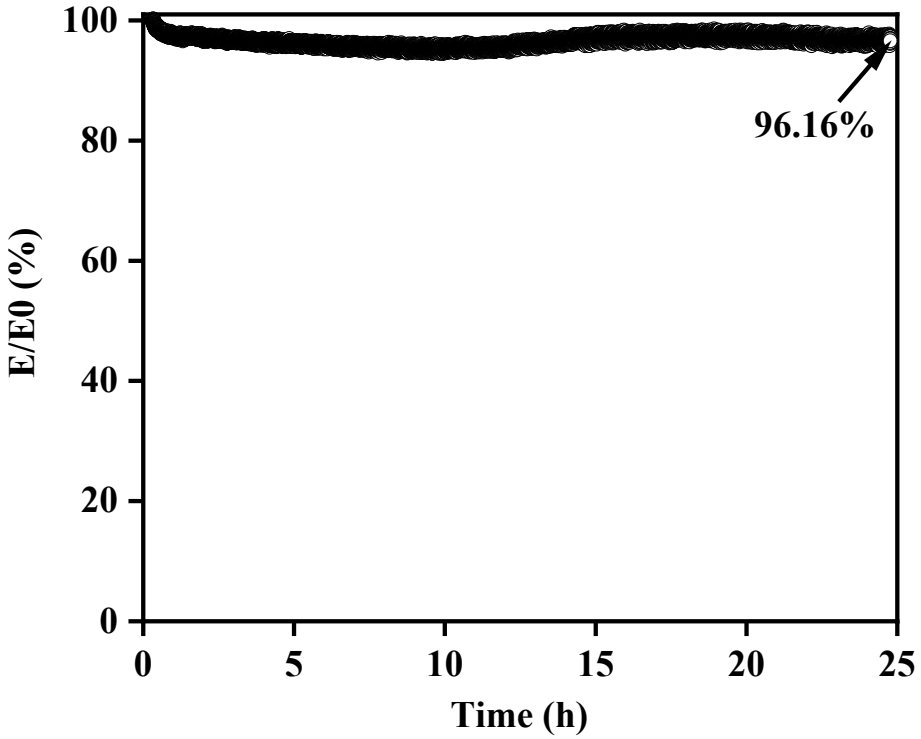

Figure S18. Durability ORR test of (CrMnFeCoNi)-P/S at a potential of 0.5 V (vs. RHE) for 25 h.

Table S1 Post-processing annealing conditions for different samples

Name	Precursor	Annealing atmosphere	Phosphorus/sulfur source
(CrMnFeCoNi)-P/S	high entropy metal precursor	N_2	sodium hypophosphite and thiourea
(MnFeCoNi)-P/S	(MnFeCoNi)-precursor	N_2	sodium hypophosphite and thiourea
(FeCoNi)-P/S	(FeCoNi)-precursor	N_2	sodium hypophosphite and thiourea
(CrMnFeCoNi)-N_2	high entropy metal precursor	N_2	---
(CrMnFeCoNi)-P	high entropy metal precursor	N_2	sodium hypophosphite
(CrMnFeCoNi)-S	high entropy metal precursor	N_2	thiourea
(CrMnFeCoNi)-O_2	high entropy metal precursor	O_2	---

Table S2 OER performance comparison between HEM-HENMC and recently reported transition metal compounds.

Catalyst	Electrolyte	Overpotential @10 mA cm^{-2} (mV)	Reference
Co-Fe-Ga-NiZn	1 M KOH	370	*Nano Res.* 2021, **15**, 4799
CoFeLaNiPt	0.1 M KOH	377	*Nat. Commun.* 2019, **10**, 2650
Ni-CoP	1.0 M KOH	362	*Appl. Catal. B: Environ.* 2023, **327**, 122444
$NiCo_2S_4$@g-C_3N_4-CNT	0.1 M KOH	330	*Adv. Mater.* 2019, **31**, 1808281
$Fe_5Co_5Mo_{15}O_{40}$	1.0 M KOH	308	*ACS Energy Lett.* 2023, **8,** 4506
HESMo	1 M KOH	303	*Small Struct.* 2023, **4**, 2300012
CrMnFeCoNi	1 M KOH	265	*Energy Storage Mater.* 2023, **58**, 287
N−NiS_2 NSs	1 M KOH	260	*ACS Catal.* 2022, **12**, 13234
CeO_2@CoS/MoS_2	1 M KOH	247	*Chem. Eng. J.* 2021, **420**, 127595
Ce-CoP	1.0 M KOH	240	*Adv. Energy Mater.* 2023, **13**, 2301162
CuS@$MoSe_2$	1.0 M KOH	236	*ACS Nano* 2022, **16**, 15425
(CrMnFeCoNi)S_x	1 M KOH	218	*Adv. Energy Mater.* 2021, **11**, 2002887
HEM-HENMC	1 M KOH	211.9	This work

Table S3 ORR performance comparison between HEM-HENMC and recently reported transition metal compounds.

Catalyst	Electrolyte	$E_{1/2}$ (V)	Reference
$LCMO_{64}$	0.1 M KOH	0.85	*Adv. Mater.* 2024, **36**, 2309266
Co_3O_4-CP-3	0.1 M KOH	0.69	*Adv. Mater.* 2024, **36**, 2405129
FeCo-MHs	1.0 M KOH	0.95	*J. Am. Chem. Soc.* 2023, **145**, 21273-21283
MFO-MS	1.0 M KOH	0.71	*J. Energy Chem.* 2024, **97**, 12-19
Co-HAT-CN-H	1.0 M KOH	0.78	*Carbon Energy* 2023, **5**, e303
LMNO-4h	0.1 M KOH	~0.8	*ACS Energy Lett.* 2024, **9**, 3440-3447
MnN/C-9	0.1 M KOH	0.87	*Nat. Mater.* 2024. DOI:10.1038/s41563-024-01998-7
HEM-HENMC	1.0 M KOH	0.84	This work